J MATER SCI 41 (2006) 697–707

Defect microstructures in epitaxial $PbZr_{0.2}Ti_{0.8}O_3$ films grown on (001) $SrTiO_3$ by pulsed laser deposition

I. B. MISIRLIOGLU, A. L. VASILIEV*, S. P. ALPAY, M. AINDOW†
Department of Materials Science and Engineering, Institute of Materials Science, University of Connecticut, Storrs, CT 06269-3136, USA
E-mail: m.aindow@uconn.edu

R. RAMESH
Department of Materials Science and Engineering and Department of Physics, University of California, Berkeley, CA 94720, USA

Transmission electron microscopy has been used to investigate the character and distribution of the microstructural features in epitaxial (001) ferroelectric $PbZr_{0.2}Ti_{0.8}O_3$ films grown on (001) $SrTiO_3$ substrates by pulsed laser deposition. The TEM observations revealed that the films were predominantly *c*-oriented with embedded a_1- and a_2-oriented domains lying on {101} planes. The substrate/film interfaces contained arrays of edge-type misfit dislocations and there were extraordinarily high densities ($\gg 10^{10}$ cm^{-2}) of threading dislocations in the films. The character and distribution of these features are consistent with the following relaxation sequence. Firstly, the lattice misfit between the phases is accommodated at the growth temperature by the introduction of misfit dislocations at the edges of island nuclei, and some of these dislocations are forced away from the interface to form threading segments upon island coalescence. Next, the film adopts the *c*-orientation upon cooling through the Curie temperature with a_1- and a_2-oriented domains being formed to ameliorate the self-strain of the transformation. Finally, some redistribution of the embedded domains and misfit dislocations occurs in response to stresses caused by expansion coefficient differences. The impact of these defects on the electrical and electromechanical properties of epitaxial ferroelectric properties is discussed.

1. Introduction

Thin films of perovskite ferroelectric materials such as $BaTiO_3$, $PbTiO_3$, and solid solutions of $PbTiO_3$-$PbZrO_3$ [$Pb(Ti_{1-x}Zr_x)O_3$ compounds, PZT] have received considerable interest because of their numerous potential device applications in micro- and nanoelectronics as elements of non-volatile random access memories (NVRAM), dynamic random access memories (DRAM), high dielectric constant capacitors, optical waveguides, tunable devices, and pyroelectric detectors. Progress in deposition techniques has made it possible to grow these ferroelectric ceramics as thin films with exceptional compositional control on a variety of different substrates. In polycrystalline ferroelectric films the grain boundaries have a detrimental effect upon the electrical properties, and the films must be poled to achieve maximum polarization, piezoelectric, pyroelectric, and electro-optic responses [1, 2]. If, however, appropriate combinations of substrate and deposition conditions are chosen, single-crystal epitaxial ferroelectric thin films can be grown, and superior physical properties can be expected [3].

Although single-crystal epitaxial ferroelectric films do not contain grain boundaries, they do exhibit a complex defect microstructure, which may include such features as twins (or poly-domains), anti-phase boundaries, interfacial misfit dislocations (MDs) and threading dislocations

Present Address: Department of Materials Science and Engineering, The Ohio State University, Columbus, OH 43210-1178, USA.
†Author to whom all correspondence should be addressed.
0022-2461
DOI: 10.1007/s10853-006-6488-9

(TDs). The evolution of this complicated microstructure is in direct response to the internal stresses that develop during film growth and subsequent cooling from the deposition temperature. These internal volumetric stresses arise due to lattice mismatch and/or thermal expansion coefficient (TEC) differences between the film and the substrate, and the self-strain of any phase transformations that occur upon cooling. In addition, there are "microstresses" which are associated with, and concentrated near, defects such as dislocations and vacancies.

Ferroelectric films are grown under conditions (temperatures/pressures) for which they are in their cubic paraelectric state. Depending on the film thickness, the epitaxial misfit strains can be reduced dramatically by the generation of interfacial MDs [4]. For deposits that grow initially as continuous pseudomorphic films in Frank/van der Merwe mode, the consensus is that MDs are introduced by nucleation of half-loops at the deposit surface. These loops expand towards the substrate/deposit interface in response to the internal stresses, and the final configuration consists of a misfit segment lying in the interfacial plane bounded by two threading segments that thread from the interface to the deposit surface [5]. For deposits that grow initially as island nuclei in Volmer/Weber mode, MDs can be introduced more easily at the periphery of the island nuclei, and TDs are formed when MDs are forced away from the interface during island coalescence. The authors have presented evidence for defect generation by these latter processes in epitaxial barium strontium titanate (BST) films on (001) $LaAlO_3$ [6].

Upon cooling, additional internal stresses will develop in epitaxial ferroelectric films both due to the differences in the TECs of the film and the substrate, and due to the self-strain of the ferroelectric phase transformation. The ferroelectric phase has a lower symmetry than the high-temperature paraelectric phase giving rise to several crystallographically equivalent transformation variants or "elastic" domains [7, 8]. In poly-domain structures the domains are twin-related and, in each case, the composition plane is parallel to the habit plane of the domain boundary. Thus, the twin domains are mechanically compatible and the interdomain interface is stress-free. After the phase transformation, a twinned film can usually give a lower effective misfit to the substrate than a single domain film. As such, the formation of a poly-domain microstructure decreases the misfit contribution to the elastic energy of an epitaxial system and is, therefore, a thermodynamically driven phenomenon. For example, in $BaTiO_3$ and $PbTiO_3$, the TiO_6 octahedra are linked in a regular cubic array forming the high-symmetry $Pm\bar{3}m$ prototype in the paraelectric state. In the ferroelectric state below the Curie transition temperature T_C (130°C and 490°C for $BaTiO_3$ and $PbTiO_3$, respectively), a spontaneous polarization arises due to the non-centrosymmetric displacement of Ti^{4+} and O^{2-} ions relative to Ba^{2+} or Pb^{2+} ions resulting in a tetragonal lattice (*P4mm*) [9]. Should this transformation occur in a constrained medium, as is the case in an epitaxial film, the formation of poly-domain structures may reduce the total energy of the system [10–15].

Over the past few years, there have been numerous experimental studies of the microstructure in ferroelectric films using transmission electron microscopy (TEM) [16–26], *in-situ* X-ray diffraction (XRD) [27, 28], and atomic force microscopy in the piezoelectric mode (*P*-AFM) [29–36]. While these studies have resulted in a generally applicable description of the microstructural evolution, they have mostly concentrated on one aspect of the defect microstructure. In this report, we present a detailed TEM and high resolution TEM (HRTEM) analysis of all aspects of the defect structure in one particular epitaxial ferroelectric system. The system is (001) $PbZr_{0.2}Ti_{0.8}O_3$ (PZT 20/80) grown by pulsed laser deposition (PLD) onto (001) $SrTiO_3$ substrates. This system was chosen because it exhibits a greater diversity of defect types than any other system we have analyzed, and previous studies have shown that both poly-domain twins and interfacial MDs can occur in the same film [23, 37, 38]. As such, this constitutes an excellent case study and enables us to investigate the interaction of the defect types. The defect configurations observed have been used to deduce the way in which the defect microstructure evolves during deposition and subsequent cooling to room temperature. The likely impacts of the various types of defects on the electrical and electromechanical properties are also discussed.

2. Experimental methods

Epitaxial PZT 20/80 films of ~300 nm in thickness were grown by PLD onto (001) single-crystal STO substrates using a 248 nm KrF excimer laser source. The growth conditions used were those that have been shown previously to result in high quality epitaxial films with the orientation: $(001)_{PZT}//(001)_{STO}$ and $[100]_{PZT}//[100]_{STO}$ [37]. Briefly, the substrates were heated to 600°C and films were deposited from a PZT 20/80 ceramic target with a pulse repetition rate of 5 Hz and an energy of 600 mJ/pulse under an O_2 partial pressure of 100 mTorr. The chamber was then back-filled with O_2 before allowing the films to cool to room temperature at a rate of 5°C per minute. Both plan-view and cross-sectional TEM specimens were prepared in the usual manner by mechanical pre-thinning followed by Ar^+ ion-beam milling to perforation in a Gatan PIPS 641 at an accelerating voltage of 3.5 kV. Plan view samples were thinned from the substrate side only: a thin glass cover slip was placed over the deposit side during milling to protect the sample surface from contamination. Microstructural analyses were performed in a JEOL JEM-2010 FasTEM equipped with an ultra-high resolution objective lens pole-piece (spherical aberration coefficient $C_s \approx 0.5$ mm) and operating at an accelerating voltage of 200 kV. In this configuration, the point-to-point resolution at Scherzer defocus is <0.19 nm.

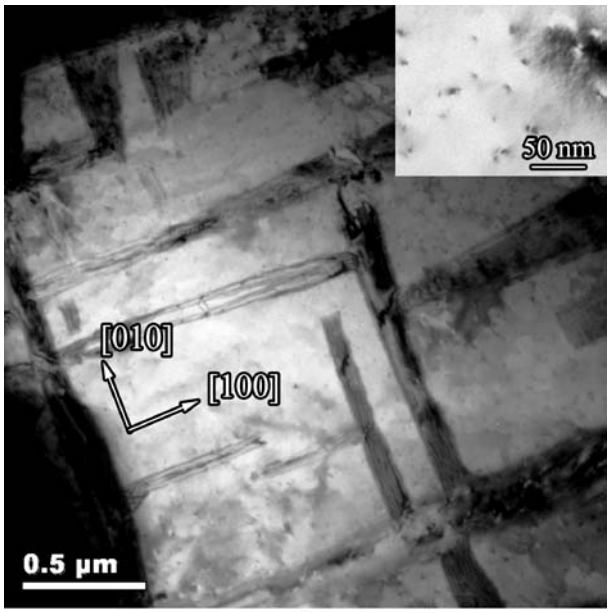

(a)

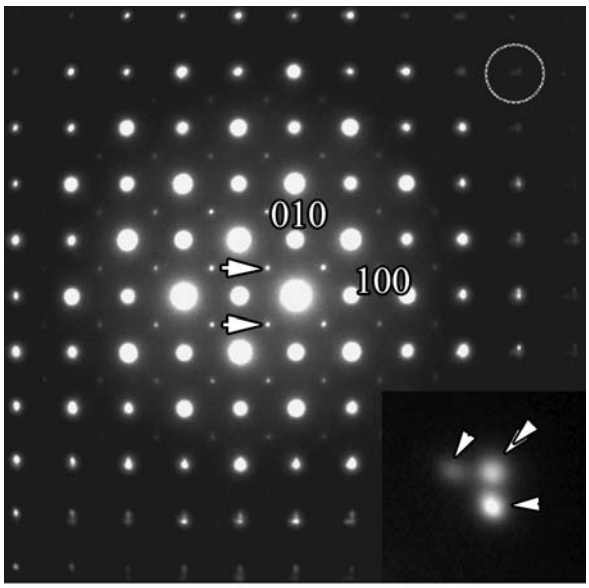

(b)

Figure 1 Data from the PZT film surface obtained at the [001] zone axis using a plan-view specimen back-thinned from the substrate side only: (a) many-beam BF image of a region containing intersecting embedded domains—a higher magnification image showing TDs in a region between the domains is inset, (b) SADP showing the main reflections from the *c*-oriented matrix together with *h*/2 *k*/2 0 superlattice reflections (examples marked by arrows)—spot splitting due to embedded a_1- and a_2-oriented domains is evident in higher order reflections as shown in the inset enlargement of the 440 matrix reflection.

3. Results

3.1. Plan-view samples

TEM data obtained from the plan-view samples confirmed that the PZT films were single-crystal and consisted mainly of *c*-axis domains. Typical data are shown in Fig. 1. Fig. 1a is an axial bright-field (BF) image obtained from an untilted plan-view sample (i.e., with the beam direction, **B**, parallel to [001]). Since these specimens were back-thinned from the substrate side only, the microstructure observed in such images corresponds to that at the PZT deposit surface. The microstructure appears to consist mainly of a single "matrix" domain with two orthogonal sets of thin embedded laths of other domains. The corresponding selected area diffraction pattern (SADP) is shown in Fig. 1b. There is no evidence for tetragonal distortion in the positions of the main peaks, indicating that for the majority of the film the *c*-axis of the tetragonal structure is perpendicular to the substrate, as expected. One of the more interesting aspects of these SADPs is the presence of pronounced intensity in $\frac{1}{2}h$, $\frac{1}{2}k$, 0 positions, and two examples are indicated by arrows in Fig. 1b. The presence of pronounced maxima at fractional positions in SADPs is usually indicative of long-range ordering. For PZT, there are several ways in which this could occur including ordering of Zr and Ti on the tetravalent cation sublattice, ordering of oxygen vacancies on the anion sublattice, or coordinated rotations of oxygen octahedra [39–42]. Further experiments are underway in an attempt to distinguish between these possibilities.

The embedded laths have lengths of up to 1 μm and lie with their major axes parallel to the [100] and [010] directions in the matrix. The laths exhibit characteristic fringe contrast at their edges with the fringes lying parallel to the major axes, indicating that the habit planes for the laths are inclined to the [001] direction in the matrix. The character of these laths was confirmed by analysis of SADPs. Careful examination of the higher order reflections revealed spot splitting as shown in the inset to Fig. 1b, which is an enlargement of the 440 matrix reflection. The positions of the satellite spots are consistent with the laths being a_1/a_2-oriented domains overlapping with the *c*-oriented matrix. We note that in some regions with a very high density of these laths (e.g., Fig. 2), occasional lath-like features were observed lying parallel to ⟨110⟩ in the matrix, usually at the intersections of packets of laths lying parallel to [100] and [010].

In regions of *c*-oriented matrix between these lath-like domains, dark/bright lobe-like strain contrast revealed the presence of high densities of TDs, as shown in the enlarged inset to Fig. 1a. From such images we estimate the density of TDs at the deposit surface to be $\approx 10^{11}$ cm^{-2}. Since most of the TDs in these films have line directions, ξ, parallel to [001], they are revealed more clearly in BF images obtained using two-beam conditions with the sample tilted several degrees away from the [001] zone axis. Three such images are shown in Fig. 3: these are part of a series of images used to identify the Burgers vectors of the TDs using diffraction contrast analysis. Four different sets of TDs are present in the films and examples of these are indicated by the letters A, B, C and D in Figs. 3(a) and (b). The TDs in sets A and D have ξ = [001] and Burgers vectors, **b**, of [010] and [100], respectively. Thus, set A

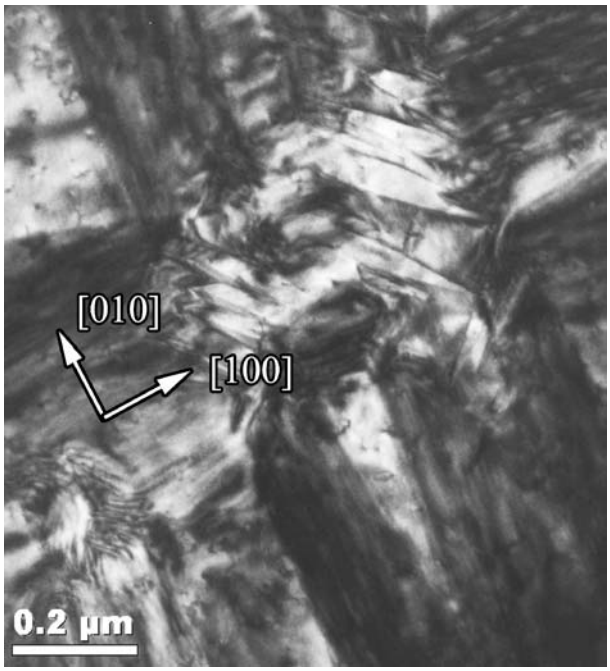

Figure 2 Many-beam BF TEM image obtained at the [001] zone axis from a back-thinned plan-view specimen showing domains oriented along $[1\bar{1}0]$ at the intersection of domains parallel to [100] and [010].

exhibits very strong contrast in Fig. 3a which was obtained using the diffraction vector $\mathbf{g} = 020$, but is out of contrast in Fig. 3b for which $\mathbf{g} = \bar{2}00$, and *vice versa* for set D. These two sets constitute the majority of the TDs in the films (>90%) but small numbers of defects from sets B and C were observed in each area. The TDs in these sets had $\xi = \langle 111 \rangle$ and $\mathbf{b} = \langle 110 \rangle$. They exhibited weaker contrast than sets A and D in images obtained using $\mathbf{g} = 020$ or $\bar{2}00$, but much stronger contrast in images obtained using $\mathbf{g} = 110$ or $1\bar{1}0$. One example is shown in Fig. 3c, which was obtained using $\mathbf{g} = 110$ from a region adjacent to that shown in Fig. 3(a) and (b). The TDs with $\mathbf{b} = [110]$ are out of contrast in this image but the configuration of those with $\mathbf{b}$=[110] is revealed more clearly. These show much more complex geometries than the straight TDs in sets A and D, including loops, half loops, and cases where ξ changes abruptly at twin boundaries.

HRTEM imaging was used to verify the values of $\mathbf{b}$ determined using diffraction contrast analysis by performing circuit mapping around the TD cores. Examples of HRTEM images obtained with $\mathbf{B} = [001]$ from TDs with $\mathbf{b} = \langle 100 \rangle$ and $\langle 110 \rangle$ are shown in Figs. 4(a) and (b), respectively. The TD shown in Fig. 4a lies next to the coherent boundary between the *c*-oriented matrix and an a_2-oriented domain. It is clear from the image that the TD has a compact core and the Burgers circuit shows that the projected component of $\mathbf{b}$, $\mathbf{b}' = [100]$. For the TD shown in Fig. 4b, however, $\mathbf{b}' = [\bar{1}\bar{1}0]$ and the core appears to be extended along the trace of (110). Circuit maps constructed around the two ends of the extended feature give $\mathbf{b}' = \frac{1}{2}[\bar{1}\bar{1}0]$ in each case, indicating that these are closely-coupled partial dislocations separated by a stacking fault approximately parallel to (110). Clearly, the apparent dissociation of such TDs could be due to projection effects since $\xi \neq [001]$. In this case, however, the displacements do appear to be localized at the ends of the extended feature. Moreover, we note that dissociations of the type:

$$[110] \rightarrow \frac{1}{2}[110] + \frac{1}{2}[110]$$

have been observed previously in a number of perovskite films [25].

3.2. Cross-sectional samples

The distribution of the defects through the film thickness was revealed more clearly in TEM images obtained from the cross-sectional samples. Fig. 5a is a typical axial BF image obtained from one such sample with $\mathbf{B} = [010]$, and Fig. 5b is the corresponding SADP. The differences in the splitting between PZT and STO peaks in the 001 and 100 systematic rows of the pattern confirm that the

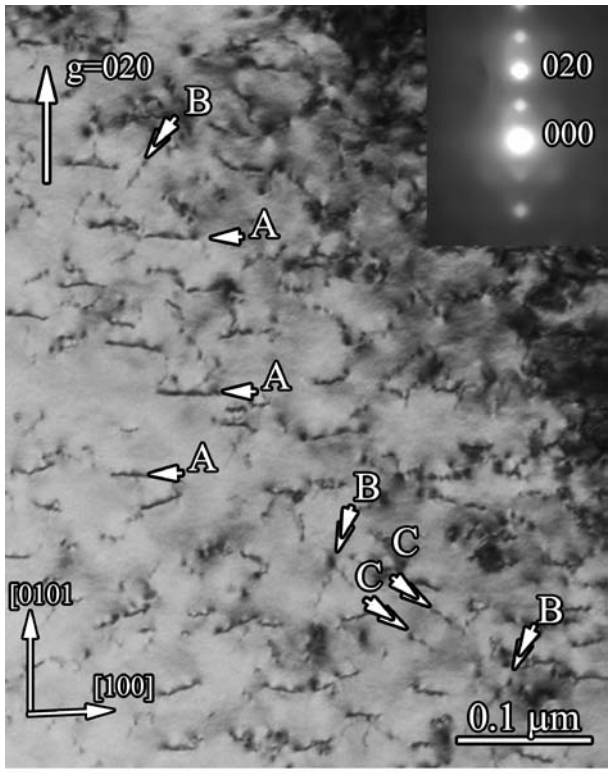

(a)

Figure 3 Two-beam BF TEM images obtained from a back-thinned plan-view specimen by tilting away from the [001] zone axis along the respective Kikuchi bands: (a) and (b) are part of a set of images obtained from the same area and used to determine the Burgers vectors of the sets of straight TDs—A, B, C and D; (c) is a region adjacent to that in (a) and (b) showing some of the other configurations of TDs with $\mathbf{b} = \langle 110 \rangle$..

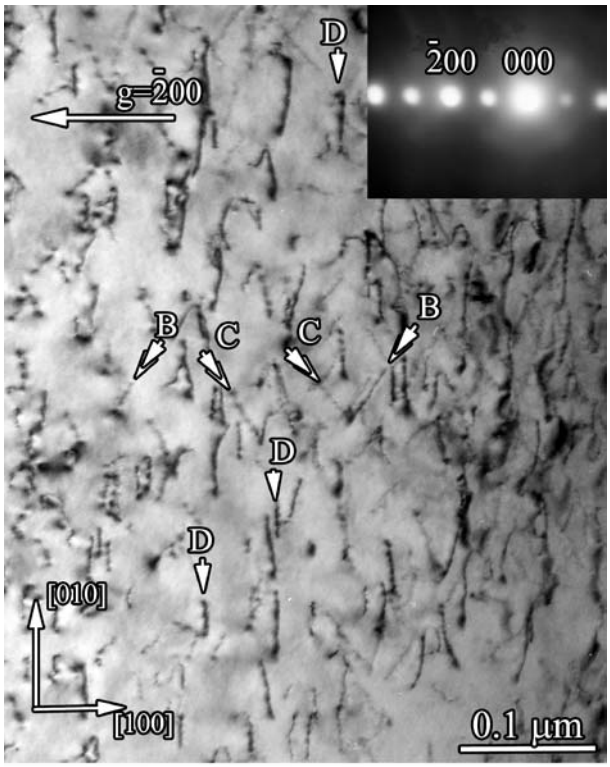

(b)

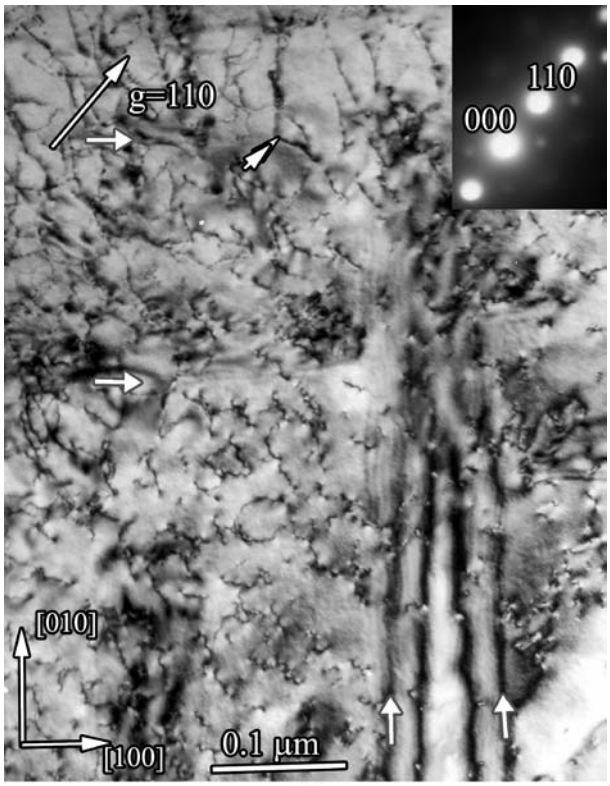

(c)

Figure 3 (Continued).

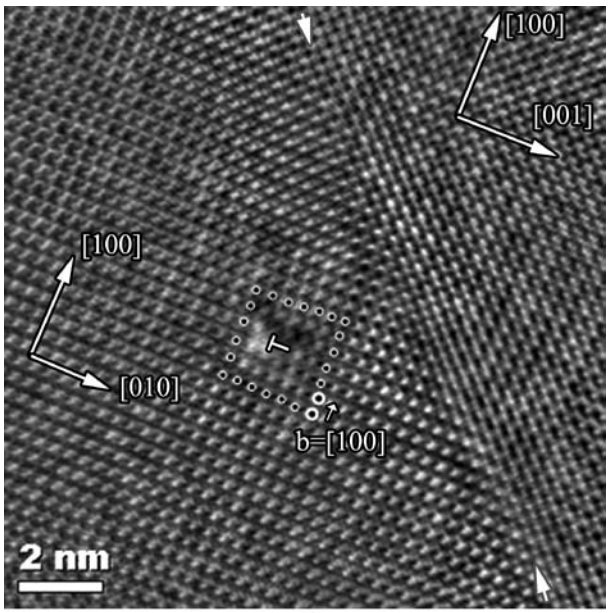

(a)

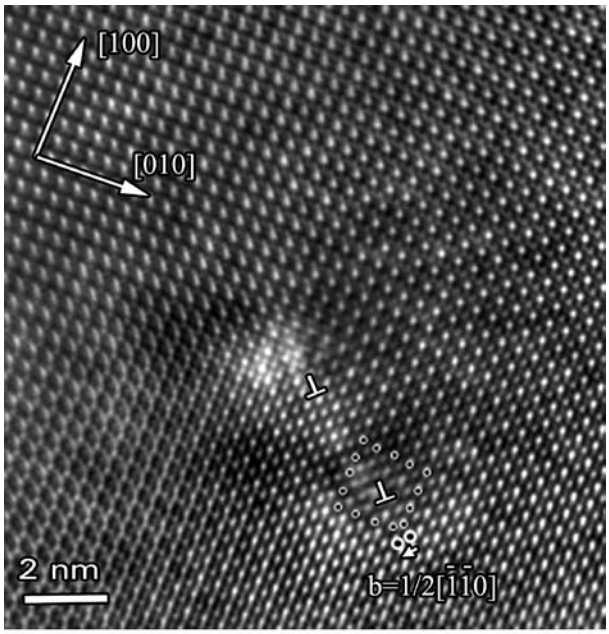

(b)

Figure 4 HRTEM images obtained at the [001] zone axis from a back-thinned plan-view TEM specimen showing examples of the two types of TDs in the film.

matrix of the film is *c*-oriented. The density, distribution and character of the TDs are consistent with those determined from the plan-view samples. Thus, the TDs are distributed uniformly with a density of $\gg 10^{10}$ cm^{-2}, most are straight and aligned with ξ = [001], and diffraction contrast analysis reveals that these have $\mathbf{b}$ = [100] or [010]. Fig. 6 is a pair of BF images obtained under two-beam conditions using $\mathbf{g} = 00\bar{2}$. The straight TDs are essentially out of contrast in these images because both $\mathbf{g}\times\mathbf{b} = 0$ and $\mathbf{g}(\mathbf{b}\times\xi) = 0$. Other configurations are

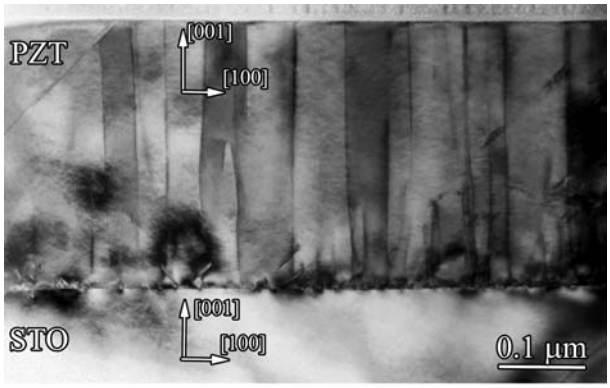

(a)

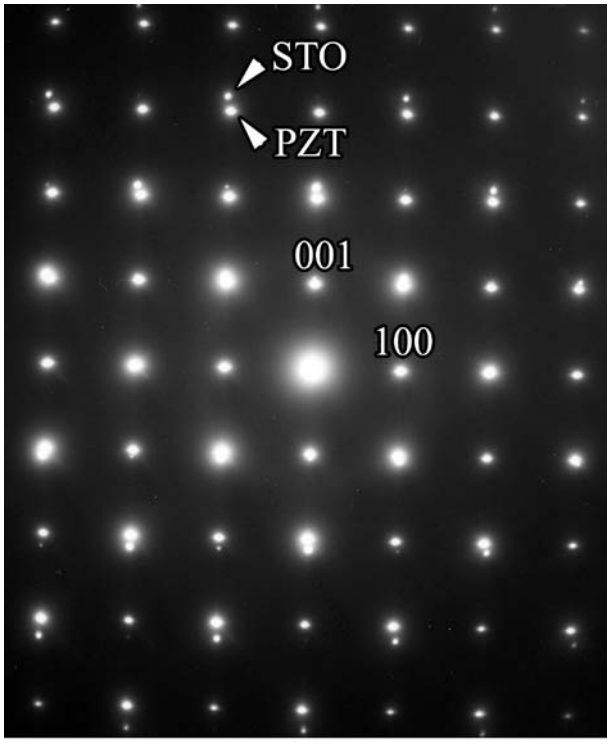

(b)

Figure 5 Data obtained from a cross-sectional specimen at the [010] zone axis: (a) many-beam BF showing straight TDs extending from the interface to the deposit surface; (b) SADP showing the superimposed zone axis patterns from the *c*-oriented PZT matrix and the STO substrate.

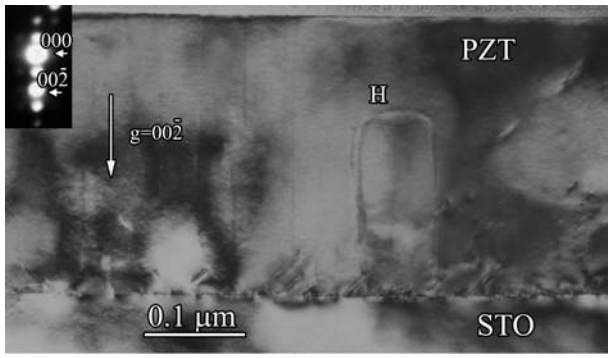

(a)

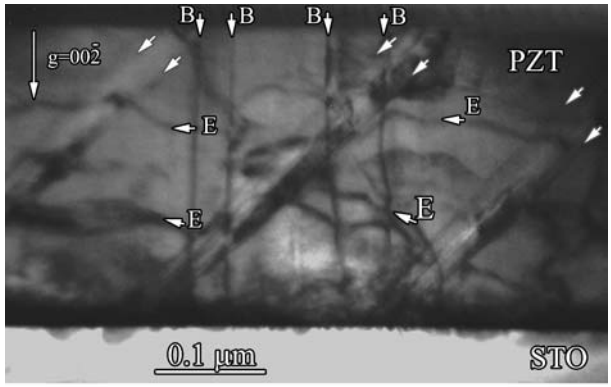

(b)

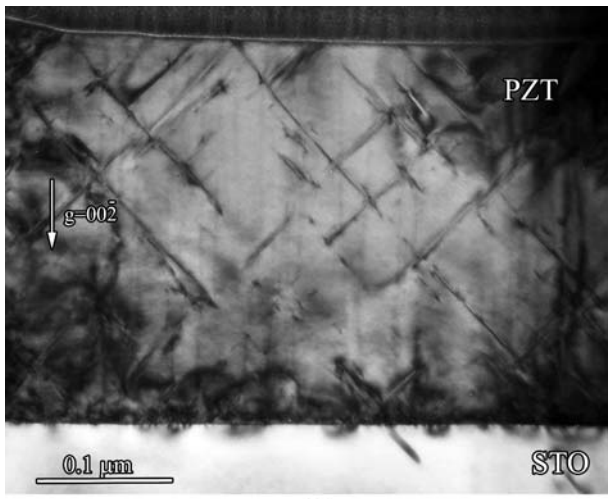

(c)

Figure 6 Two-beam BF TEM images obtained from cross-sectional specimens by tilting away from the [010] zone axis along the 002 Kikuchi band showing: (a) residual contrast from a TD half-loop (marked H); (b) a thicker region with more complex contrast arising from inclined domains (arrowed) lying on ($\bar{1}$01), straight TDs (marked B) and half-loop-type features (marked E); (c) a region containing inclined domains lying on($\bar{1}$01) and (101).

observed, however. Occasionally "residual" $\mathbf{g}(\mathbf{b}\times\xi)$ contrast was present from dislocation half-loops and one example is marked H in Fig. 6a. Interestingly, the curvature of these half-loops suggests that they are emanating from the interface and propagating towards the deposit surface, and not *vice versa* as one might expect. Fig. 6b was obtained from a significantly thicker region of the TEM sample and, as such, the contrast is more complex because the kinematical conditions for straightforward diffraction contrast analysis are not met. Thus, the straight TDs marked B give rise to appreciable contrast despite the orientation of **g**. Nonetheless, here again there are dislocations in the film whose curvature indicates that they are propagating towards the deposit surface (marked E). These features also undergo changes in curvature when they impinge upon the TDs and the inclined boundaries of a_1- or a_2-oriented domains (indicated by white arrows on the Figure). The domain boundaries appear edge-on and

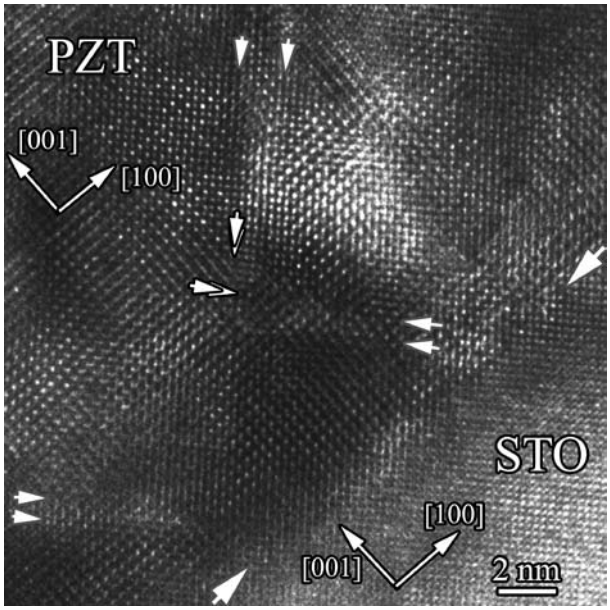

Figure 7 HRTEM image obtained at the [010] zone axis from a cross-sectional specimen showing intersecting micro-domains at the PZT/STO interface.

have [101] traces in this micrograph. Thus the habit plane is $(\bar{1}01)$, which is consistent with the observations from the plan-view samples. We note that there is a pronounced local anisotropy in the region shown in Fig. 6b: there are domains on $(\bar{1}01)$ but not on (101). In other areas, such as that shown in Fig. 6c, there are domains on both $(\bar{1}01)$ and (101), but all areas showed both some anisotropy in the domain populations and a decrease in the number density of domains with increasing distance from the STO/PZT interface.

The details of the defect microstructure in the region of the STO/PZT interface were investigated using HRTEM. One such image is shown in Fig. 7 and we note that the quality of such images is poorer than those obtained from other regions due to the complexity of the strain state. A very high density of ultra-thin ($\approx$1 nm) microdomains was observed (marked with white arrows). These lay on $(\bar{1}01)$ and (101), with most of them originating at MDs, and terminating within 20–30 nm of the interface at intersections with other microdomains or at dislocations [43] with $\mathbf{b} = 1/2\langle 101\rangle$ (two examples are marked with double arrowheads). Further details of the dislocation structure at the interface was revealed by Fourier-filtering of HRTEM images to reduce the effects of strain and three examples are shown in Fig. 8. The majority of the dislocations are edge-type with **b** equal to a lattice translation vector. They are revealed most clearly in the largest a_1- or a_2-oriented domains: two examples are shown in Fig. 8a and for both of these $\mathbf{b} = [001]$. It is interesting to note that there appears to be a small "standoff" with the dislocations lying 1–2 nm above the PZT/STO interface. Occasional dislocations were also observed with $\mathbf{b} = 1/2\langle 101\rangle$. These lay

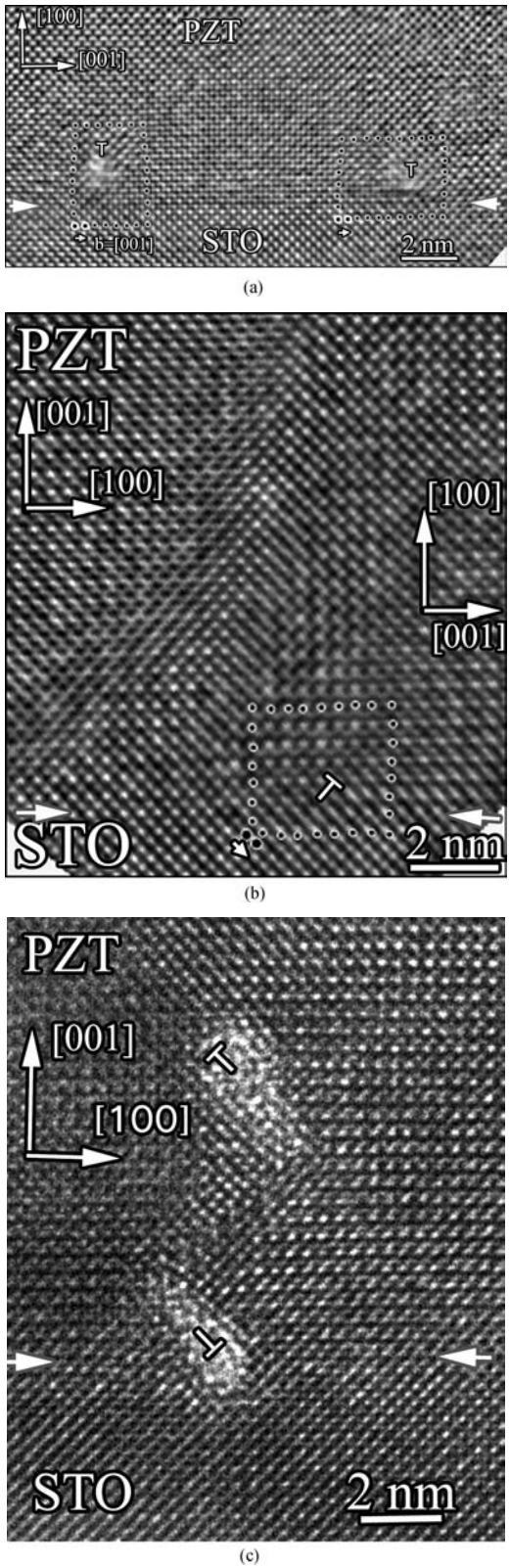

Figure 8 Fourier-filtered HRTEM image obtained at the [010] zone axis of STO from cross-sectional specimens at the PZT/STO interface showing: (a) edge-type MDs lying just above the interface; (b) a dislocation with $\mathbf{b} = 1/2\langle 101\rangle$ at the intersection of an a_1-oriented domain with the interface; (c) a pair of dislocations with $\mathbf{b} = \pm 1/2\langle 101\rangle$ at either end of a short microdomain.

either at the triple lines where inter-domain boundaries met the PZT/STO interface as shown in Fig. 8b, or at either end of short micro-domain segments as shown in Fig. 8c.

4. Discussion

In this section we consider firstly the way in which the observed defect microstructure might develop and then describe the influence that these defects would have upon the electrical properties of the films.

4.1. Microstructural development

One of the most significant influences on the defect microstructure is the lattice misfit between the deposit and the substrate. No accurate data are available for the lattice parameters at the deposition temperature, but these have been estimated previously as 0.4001 and 0.3932 nm for the paraelectric cubic phase of PZT 20/80 and for STO, respectively [37]. This would give a lattice misfit of 1.75% during epitaxial deposition. As such, one would expect the PZT deposits to form initially as islands growing in the 3D Volmer-Weber mode. In this mode, edge-type MDs are usually introduced periodically at the periphery of the growing islands to minimize the strain in the deposit. This would give orthogonal arrays of MDs with $\mathbf{b} = [100]$ or [010] as observed here (e.g. Fig. 8a). To explain the high densities of TDs, we recall some of the earliest work on epitaxy of metals, wherein it was shown that TDs can form when adjacent islands which are misaligned and/or misoriented with respect to one another coalesce [44]. This results in some of the MDs being forced away from the interface. Studies on other heteroepitaxial oxide on oxide systems grown by PLD have shown that islands with substantial misorientations can be deposited whilst still resulting in single-crystal epitaxial films after coalescence [45]. Thus, if the density of island nuclei were high enough, and coalescence were to occur at an early stage in the growth, then a high density of TDs could arise with Burgers vectors parallel to the interface, as observed experimentally. At densities of $>10^{10}$ cm^{-2} the distance between the TDs is low enough that the magnitudes of elastic interactions between adjacent threading segments will be significant. Where the forces between these segments are attractive, the interaction would lead to the combination or mutual annihilation of adjacent segments, giving a decrease in TD density with increasing film thickness. Due to the complexity of the final microstructure, we have not been able to determine whether or not such a reduction does occur. We note, however, that the small proportion ($<10\%$) of TDs with $\mathbf{b} = \langle 110 \rangle$ (sets B and C in Fig. 3) could arise due to the combination of TDs with $\mathbf{b} = \pm[100]$ and $\mathbf{b} = \pm[010]$.

Upon cooling, additional stresses may develop in the film due to both TEC mismatch and the self-strain of the phase transformation. The mean TEC for PZT 20/80 above the Curie temperature ($T_C \approx 450$°C) is $\approx 15 \times 10^{-6}$ °C^{-1}, whereas the value for STO is 11×10^{-6} °C^{-1}. As such, the TEC mismatch strain produced on cooling from the growth temperature to T_C will be 0.08% and the corresponding stresses will be *tensile*, i.e., in the opposite sense to the misfit stresses at the growth temperature. Since the magnitude of the TEC mismatch strain is small, it could be accommodated elastically. The TD density is, however, certainly high enough for the MD content to be modified by the lateral glide of TDs in the manner described by Matthews and co-workers [46].

Upon cooling through T_C PZT undergoes a transformation from the cubic paraelectric phase to the tetragonal ferroelectric phase. The lattice parameters for PZT 20/80 just above and below T_C have been estimated as: $a_{(451°C)} = 0.3989$ nm, $a_{(449°C)} = 0.3977$ nm, and $c_{(449°C)} = 0.4023$ nm [37]. Thus, one would expect the transformation stresses to be somewhat higher for a_1- or a_2-oriented domains than for c-oriented domains, which may help to explain why the c-orientation constitutes the matrix of the film. If one assumes that the stresses due to lattice misfit are fully relaxed by MDs just above the transformation temperature, then the transformation stresses will also be *tensile*. These stresses can be accommodated, at least in part, by the introduction of a_1- or a_2-oriented domains [47]. The stress state in a_1- or a_2-oriented domains will be mixed with a compressive component parallel to the c axis of the domain and a tensile component parallel to a_2 or a_1, respectively. As such, a combination of a_1- and a_2-oriented domains could help to accommodate the transformation stresses in the c-oriented matrix. The HRTEM data obtained here indicate that these domains nucleate at MDs in the PZT/STO interface and propagate into the film on $\{101\}$ habit planes, in accordance with theoretical predictions [48]. The number density of these domains decreases rapidly, with the vast majority terminating within a few nm of the interface at intersections with other domains. In many areas this process leads to the development of an anisotropic population in the domains. It is tempting to speculate that this bias in the population could be due to small vicinal deviations from the nominal (001) substrate surface orientation as observed previously for yttrium barium copper oxide on (011) STO [49]. In the present case a vicinal surface could arise due to unintentional surface offcut or locally due to surface roughness.

Significant additional stresses can develop in the films upon cooling from T_C to room temperature due to TEC mismatch. The TEC for PZT over this temperature range is highly anisotropic with average values of $\approx 25 \times 10^{-6}$ °C^{-1} in the (001) plane and $\approx 64 \times 10^{-6}$ °C^{-1} in the c direction. For the single-crystal c-oriented films considered here, the TEC mismatch strain that would develop on cooling from T_C to room temperature is $\approx 0.6\%$, and this will give significant additional *tensile* stresses in the PZT film. These stresses could be alleviated somewhat

by the formation of additional a_1- or a_2-oriented domains or by the growth of the ones introduced in response to the transformation stresses. An alternate mechanism is, however, suggested by the dislocation arrangements shown in Fig. 6. If the misfit and transformation stresses were accommodated completely by the MDs and a_1- and a_2-oriented domains just below T_C then the effects of TEC mismatch could be ameliorated by the elimination of some of the MDs from the PZT/STO interface. Given that the MDs have $\mathbf{b} = [100]$ or [010], this would have to occur by climb rather than glide, but it would account for the dislocations which appear to be emanating from the interface and bowing out until they are impeded by inclined domains and/or TDs (Fig. 6). It is also conceivable that such processes might account for the 1-2 nm "standoff" between the MDs and the interface.

4.2. Effect of microstructure upon ferroelectric properties

Many of the useful properties of ferroelectrics including the high piezo- and pyroelectric responses are of "extrinsic" nature, i.e., they are related to reversible domain wall movements of the poly-domain structure in response to changes in external conditions such as variations in the temperature, the stress, or the applied electric field. This extrinsic contribution may be an order of magnitude larger than the intrinsic response due to relative displacements of ions in the ferroelectric lattice, in particular for "hard" ferroelectrics such as $PbTiO_3$ and Ti-rich PZT with a high tetragonality (i.e., the c/a ratio) [1]. If ferroelectric materials are deposited as films on a thick substrate, the substrate will essentially clamp the film and prevent it from deforming in the presence of an applied field [50], thus resulting in weaker intrinsic dielectric, pyroelectric, and piezoelectric responses [51–55]. Moreover, the internal stresses will result in a shift of the phase transformation temperature that will decrease or increase the strength of the intrinsic electrical and electromechanical responses depending on whether the in-plane stress state is tensile or compressive [56].

Theoretical estimates show that extremely high ferroelectric coefficients can be expected in epitaxial ferroelectric films with a poly-domain structure if the domain walls are mobile [57]. However, should a poly-domain state form in an epitaxial ferroelectric film, microstresses will be generated at the film-substrate interface due to the periodic deviation of the actual misfit from the average misfit [58]: this will certainly inhibit the movement of domain boundaries under the influence of an applied external field. Furthermore, as shown in this study, the domains emanate from MDs that have formed at the deposition temperature. The domains are, therefore, pinned due to the microstresses around the MD cores. The low mobility of the domain walls has been verified experimentally via *in situ* XRD wherein the domain fractions of poly-domain epitaxial ferroelectric films were not affected significantly by an applied electric field [59]. Furthermore, *P*-AFM results indicate that the domain structures of ferroelectric films do not change even in the presence of highly localized electric fields [38]. However, we note that experimental measurements of the domain fractions in $PbTiO_3$ and Ti-rich PZT show that the poly-domain structure is extremely sensitive to variations in the temperature [10, 14, 27, 47, 60]. This clearly suggests that the relaxation kinetics are extremely sluggish since the relaxation times involved in temperature dependence experiments are inevitably far greater than those in electrical measurements, which are performed at frequencies of $\gg 1$ Hz. Therefore, we can conclude that a poly-domain microstructure in epitaxial ferroelectric films results in inferior electrical and electromechanical responses as compared with bulk material, due to the clamping effect of the substrate and the immobilization of the domain walls due to the highly localized stresses at the film-substrate interfaces.

The MDs that relieve the internal stresses at the growth temperature have another detrimental effect. Recently, we have carried out a preliminary thermodynamic analysis on the effect of dislocations in ferroelectric materials [61] that was supported by polarization hysteresis, dielectric, and piezoelectric measurements [62, 63]. It was shown that there is a drastic variation in the polarization near the dislocation due to the coupling with the stress field of the dislocation. These polarization gradients result in strong depoling fields that suppress the polarization in a region that might extend over several nanometers [64], giving rise to the formation of dead layers that severely degrade ferroelectric properties [65]. These findings have significant implications in terms of the properties of ferroelectric films. Firstly, these regions may serve as pinning centers for reversible domain wall motion in the presence of an applied field, as mentioned previously. Secondly, there exists a volume within the ferroelectric film that will not contribute to the polarization, dielectric, piezoelectric, and pyroelectric responses. Furthermore, because of this dead layer, the applied electrical field that is necessary to activate the unique properties of ferroelectrics will essentially be screened. The detrimental effect of such regions is dependent on the thickness of the ferroelectric film and will obviously be enhanced in ultra-thin films. Similar conclusions can be drawn for vacancies in ferroelectric films due to their stress fields that couple with the polarization, resulting in localized polarization variations.

Based on the discussion above, it is clear that for device applications in micro- or nanoelectronics a ferroelectric film would ideally exhibit a mono-domain structure with no defects. Although it might, in principle, be possible to produce a defect-free pseudomorphic film by careful selection of deposition conditions, the clamping effect of the substrate might still result in a substantial reduction in the intrinsic response [50]. There are three main ways

in which this problem can be addressed. Firstly, one can manipulate the degree of constraint in a pseudomorphic deposit by modifying the film or substrate geometry [51]. For example, post-deposition patterning of ferroelectric epitaxial films through the film thickness to give "nanostripes" or "nanopillars" with a width less than the film thickness would effectively eliminate the constraint in certain directions. P-AFM studies of patterned epitaxial ferroelectric films indicate that this is indeed the case, resulting in a significant improvement in the electromechanical response [51, 66]. Secondly, one could use post-deposition annealing of relaxed films or ultra-thin buffer layers to give final microstructures with vastly reduced TD densities. Such films would obviously still contain MD arrays at the interface but the associated dead layers would be confined to the region at or near the interface. Finally, we note that most of these issues could be avoided by using a lattice-matched substrate but, to date, no economically viable substrate materials have been identified.

5. Summary

The defect microstructures in epitaxial PZT films grown on (001) STO substrates by PLD have been investigated using TEM and HRTEM. The character and distribution of the features has been used to infer that they are introduced into the films to relieve internal stresses according to the following relaxation sequence:

- Firstly, the para-electric cubic phase of PZT is deposited upon the STO substrate in Volmer/Weber island-growth mode. The lattice mismatch is accommodated at the growth temperature by arrays of edge-type MDs with $\mathbf{b} = \langle 100 \rangle$. These are introduced at the periphery of the growing island nuclei and a high density of TD segments is formed during coalescence of misoriented islands when MD segments are deflected out of the interface plane. Interactions of the closely-spaced TDs leads to annihilation of some segments and the combination of others to give TDs with $\mathbf{b} = \langle 110 \rangle$.
- Small TEC mismatch stresses develop upon cooling to T_C: these are accommodated elastically or by the glide of TDs to modify the MD content in the PZT/STO interface.
- Upon cooling through T_C the cubic PZT transforms to the tetragonal ferroelectric structure and the film adopts the *c*-orientation. The resultant transformation stresses are relieved by the introduction of a_1- or a_2-oriented domains, which nucleate at the MDs. These domains lie parallel to $\{101\}$ and their number reduces rapidly with distance from the interface as most terminate at intersections with other domains. Only a small proportion of the a_1- or a_2-oriented domains propagate into the film and in many cases a profound local anisotropy results due to substrate vicinality.
- Significant TEC mismatch stresses develop during cooling from T_C to room temperature and these are alleviated in part by a re-arrangement of the a_1/a_2-oriented domains and MDs. In the latter case this occurs by climb processes giving dislocation half-loops with $\mathbf{b} = \langle 100 \rangle$, which emanate from the interface and propagate towards the interface until their progress is blocked by TDs or a_1/a_2-oriented domains.

Such defects can have a profound and detrimental effect on properties of ferroelectric thin films. Observations such as those presented here highlight the pressing need for defect reduction or avoidance strategies in such systems.

Acknowledgements

This work was supported by the National Science Foundation (NSF) under Grants DMR-0132918 (I.B.M and S.P.A.), NSF-MRSEC DMR-0080008 (R.R.), and an NSF US-Europe program DMR-0244288 (R.R.).

References

1. D. DAMJANOVIC, *Rep. Prog. Phys.* **61** (1998) 1267.
2. R. RAMESH, W. K. CHAN, B. WILKENS, H. GILCHRIST, T. SANDS, J. M. TARASCON, V. G. KERAMIDAS, K. FORK, J. LEE and A. SAFARI, *Appl. Phys. Lett.* **61** (1992) 1537.
3. J. S. SPECK, A. SEIFERT, W. POMPE and R. RAMESH, *J. Appl. Phys.* **76** (1994) 477.
4. J. W. MATTHEWS and A. E. BLAKESLEE, *J. Cryst. Growth* **27** (1974) 118.
5. J. W. MATTHEWS, *J. Vac. Sci. Technol.* **12** (1975) 126.
6. I. B. MISIRLIOGLU, A. L. VASILIEV, M. AINDOW, S. P. ALPAY and R. RAMESH, *Applied Physics Letters* **84** (2004) 1742.
7. A. L. ROITBURD, *Phys. Stat. Sol. (a)* **37** (1976) 329.
8. S. LITTLE and A. ZANGWILL, *Phys. Rev. B* **49** (1994) 16659.
9. F. JONA and G. SHIRANE, "Ferroelectric Crystals" (Pergamon, New York, 1962).
10. B. S. KWAK, A. ERBIL, J. D. BUDAI, M. F. CHRISHOLM, L. A. BOATNER and B. J. WILKENS, *Phys. Rev. B* **49** (1994) 14865.
11. J. S. SPECK and W. POMPE, *J. Appl. Phys.* **76** (1994) 466.
12. N. A. PERTSEV and A. G. ZEMBILGOTOV, *ibid.* **80** (1996) 6401.
13. N. SRIDHAR, J. M. RICKMAN and D. J. SROLOVITZ, *Acta Mater.* **44** (1996) 4085.
14. S. P. ALPAY and A. L. ROYTBURD, *J. Appl. Phys.* **83** (1998) 4714.
15. Y. L. LI, S. Y. HU, Z. K. LIU and L. Q. CHEN, *Applied Physics Letters* **78** (2001) 3878.
16. Y. GAO, G. BAI, K. L. MERKLE, Y. SHI, H. L. M. CHANG, Z. SHEN and D. J. LAM, *J. Mater. Res.* **8** (1993) 145.
17. S. G. GHONGE, E. GOO and R. RAMESH, *Appl. Phys. Lett.* **62** (1993) 1742.
18. S. STEMMER, S. K. STREIFFER, F. ERNST and M. RUHLE, *Philos. Mag. A* **71** (1995) 713.
19. S. STEMMER, S. K. STREIFFER, F. ERNST, M. RUHLE, W. Y. HSU and R. RAJ, *Solid State Ionics* **75** (1995) 43.

20. B. A. TUTTLE, T. J. HEADLEY, H. N. AL-SHAREEF, J. A. VOIGT, M. RODRIGUEZ, J. MICHAEL and W. L. WARREN, *J. Mater. Res.* **11** (1996) 2309.
21. T. SUZUKI, Y. NISHI and M. FUJIMOTO, *Philos. Mag. A* **79** (1999) 2461.
22. S. HONG, E. L. COLLA, E. KIM, D. V. TAYLOR, A. K. TAGANTSEV, P. MURALT, K. NO and N. SETTER, *J. Appl. Phys.* **86** (1999) 607.
23. A. L. ROYTBURD, S. P. ALPAY, L. A. BENDERSKY, V. NAGARAJAN and R. RAMESH, *ibid.* **89** (2001) 553.
24. C. J. LU, L. A. BENDERSKY, K. CHANG and I. TAKEUCHI, *Philosophical Magazine* **83** (2003) 1565.
25. C. J. LU, L. A. BENDERSKY, K. CHANG and I. TAKEUCHI, *J. Appl. Phys.* **93** (2003) 512.
26. H. P. SUN, W. TIAN, X. Q. PAN, J. H. HAENI and D. G. SCHLOM, *Appl. Phys. Lett.* **84** (2004) 3298.
27. Y. M. KANG and S. BAIK, *J. Appl. Phys.* **82** (1997) 2532.
28. D. D. FONG, C. THOMPSON, S. K. STREIFFER, J. A. EASTMAN, O. AUCIELLO, P. H. FUOSS and G. B. STEPHENSON, *Annalen Der Physik* **13** (2004) 27.
29. A. GRUVERMAN, O. AUCIELLO and H. TOKUMOTO, *Annual Review of Materials Science* **28** (1998) 101.
30. G. ZAVALA, J. H. FENDLER and S. TROLLIER-MCKINSTRY, *J. Appl. Phys.* **81** (1997) 7480.
31. O. AUCIELLO, A. GRUVERMAN, H. TOKUMOTO, S. A. PRAKASH, S. AGGARWAL and R. RAMESH, *MRS Bulletin* **23** (1998) 33.
32. J. A. CHRISTMAN, R. R. WOOLCOTT JR., A. I. KINGON and R. J. NEMANICH, *Appl. Phys. Lett.* **73** (1998) 3851.
33. E. L. COLLA, S. HONG, D. V. TAYLOR, A. K. TAGANTSEV, N. SETTER and K. NO, *ibid.* **72** (1998) 2763.
34. E. L. COLLA, D. V. TAYLOR, A. K. TAGANTSEV and N. SETTER, *ibid.* **72** (1998) 2478.
35. C. S. GANPULE, V. NAGARAJAN, H. LI, A. S. OGALE, D. E. STEINHAUER, S. AGGARWAL, E. WILLIAMS, R. RAMESH and P. DE WOLF, *ibid.* **77** (2000) 292.
36. C. S. GANPULE, V. NAGARAJAN, B. K. HILL, A. L. ROYTBURD, E. D. WILLIAMS, R. RAMESH, S. P. ALPAY, A. ROELOFS, R. WASER and L. M. ENG, *J. Appl. Phys.* **91** (2002) 1477.
37. S. P. ALPAY, V. NAGARAJAN, L. A. BENDERSKY, M. D. VAUDIN, S. AGGARWAL, R. RAMESH and A. L. ROYTBURD, *ibid.* **85** (1999) 3271.
38. C. S. GANPULE, V. NAGARAJAN, S. B. OGALE, A. L. ROYTBURD, E. D. WILLIAMS and R. RAMESH, *Appl. Phys. Lett.* **77** (2000) 3275.
39. J. RICOTE, D. L. CORKER, R. W. WHATMORE, S. A. IMPEY, A. M. GLAZER, J. DEC and K. ROLEDER, *Journal of Physics-Condensed Matter* **10** (1998) 1767.
40. J. F. SCOTT and M. DAWBER, *Appl. Phys. Lett.* **76** (2000) 3801.
41. R. S. K. MISHRA, D. PANDEY, H. LEMMENS and G. VAN TENDELOO, *Phys. Rev. B* **64** (2001) 054104.
42. B. NOHEDA, L. WU and Y. ZHU, *ibid.* **66** (2002) 060103.
43. Z. R. DAI, Z. L. WANG, X. F. DUAN and J. ZHANG, *Appl. Phys. Lett.* **68** (1996) 3093.
44. M. J. STOWELL, in "Epitaxal Growth," edited by J. W. Matthews, (Academic Press: New York, 1975) p. 437.
45. S. J. PENNYCOOK, M. F. CHISOLM, D. E. JESSON, R. FEENSTRA, S. ZHU, X. Y. ZHENG and D. J. LOWNDES, *Physica C* **202** (1992) 1.
46. J. W. MATTHEWS, in "Epitaxal Growth," edited by J. W. Matthews, (Academic Press: New York, 1975) p. 559.
47. S. P. ALPAY, A. S. PRAKASH, S. AGGARWAL, P. SHUK, M. GREENBLATT, R. RAMESH and A. L. ROYTBURD, *Scripta Mater.* **39** (1998) 1435.
48. S. Y. HU, Y. L. LI and L. Q. CHEN, *J. Appl. Phys.* **94** (2003) 2542.
49. A. L. VASILIEV, D. S. LINEHAN, E. P. KVAM, L. HOU and M. W. MCELFRESH, *Physica C* **289** (1997) 243.
50. N. A. PERTSEV, A. G. ZEMBILGOTOV and A. K. TAGANTSEV, *Phys. Rev. Lett.* **80** (1998) 1988.
51. A. L. ROYTBURD, S. P. ALPAY, V. NAGARAJAN, C. S. GANPULE, S. AGGARWAL, E. D. WILLIAMS and R. RAMESH, *ibid.* **85** (2000) 190.
52. Z.-G. BAN and S. P. ALPAY, *J. Appl. Phys.* **91** (2002) 9288.
53. Z.-G. BAN and S. P. ALPAY, *Appl. Phys. Lett.* **82** (2003) 3499.
54. A. SHARMA, Z.-G. BAN, S. P. ALPAY and J. V. MANTESE, *J. Appl. Phys.* **95** (2004) 3618.
55. A. SHARMA, Z.-G. BAN, S. P. ALPAY and J. V. MANTESE, *Applied Physics Letters* **85** (2004) 985.
56. N. A. PERTSEV, V. G. KOUKHAR, R. WASER and S. HOFFMANN, *ibid.* **77** (2000) 2596.
57. N. A. PERTSEV, G. ARLT and A. G. ZEMBILGOTOV, *Phys. Rev. Lett.* **76** (1996) 1364.
58. A. L. ROYTBURD, *J. Appl. Phys.* **83** (1998) 239.
59. K. S. LEE, Y. K. KIM, S. BAIK, J. KIM and I. S. JUNG, *Appl. Phys. Lett.* **79** (2001) 2444.
60. C. M. FOSTER, G. R. BAI, R. CSENCSITS, J. VETRONE, R. JAMMY, L. A. WILLS, E. CARR and J. AMANO, *J. Appl. Phys.* **81** (1997) 2349.
61. S. P. ALPAY, I. B. MISIRLIOGLU, V. NAGARAJAN and R. RAMESH, *Appl. Phys. Lett.* **85** (2004) 2044.
62. V. NAGARAJAN, C. L. JIA, H. KOHLSTEDT, R. WASER, I. B. MISIRLIOGLU, S. P. ALPAY and R. RAMESH, *ibid.* **86** (2005) 192910.
63. C. L. CANEDY, H. LI, S. P. ALPAY, L. SALAMANCA-RIBA, A. L. ROYTBURD and R. RAMESH, *ibid.* **77** (2000) 1695.
64. A. M. BRATKOVSKY and A. P. LEVANYUK, *Phys. Rev. B* **66** (2002) 184109.
65. *Idem.*, *ibid.* **63** (2001) 132103.
66. C. S. GANPULE, A. STANISHEVSKY, S. AGGARWAL, J. MELNGAILIS, E. WILLIAMS, R. RAMESH, V. JOSHI and C. P. DE ARAUJO, *Appl. Phys. Lett.* **75** (1999) 3874.